PHILOSOPHICAL TRANSACTIONS OF THE ROYAL SOCIETY A MATHEMATICAL, PHYSICAL & ENGINEERING SCIENCES

# Ship capsizing analysis using advanced hydrodynamic modelling

E. Kreuzer and M. Wendt

*Phil. Trans. R. Soc. Lond. A* 2000 **358**, 1835-1851
doi: 10.1098/rsta.2000.0617

# Ship capsizing analysis using advanced hydrodynamic modelling

By E. Kreuzer and M. Wendt

*Arbeitsbereich Meerestechnik II—Mechanik, Technische Universität Hamburg–Harburg, D-21071 Hamburg, Germany*

A ship's stability is fundamental to the safety of its crew, its cargo, and the environment. Several ocean-going vessels are lost due to instability each year, particularly in high seas. To prevent such losses, a better understanding of ship stability is necessary. In this paper we analyse the stability of ships using advanced mathematical models and methods. All the rigid-body motions of a ship, as well as memory effects in the fluid, are accounted for. The analysis shows that a ship's dynamics depend strongly on the nonlinearities of the ship–fluid system. In our analysis of a particular ship, we notice a sequence of bifurcations when wave heights increase, and we believe that this is an explanation for capsizing. Critical wave heights for capsize were identified. In quartering seas, the required wave height was much lower compared with following seas. A path-following method to determine the stability limits in a systematic manner is being developed.

**Keywords: ships; stability; capsizing**

## 1. Introduction

Each year, almost 100 ships of tonnage greater than 500 GT (gross tonnage) are lost in the world's oceans (figure 1). This corresponds to a total tonnage of up to 1 000 000 GT. As a result of these accidents, 300–1400 lives are lost each year. Economical and environmental risks are of course important; but much more important is the danger to human life. Thus, it is necessary to target research at improving the tools for analysis and prediction of ships' motions in severe seas.

Both the numbers of losses and the reasons, where known, for them are collected (The Institute of London Underwriters 1997). At least one-third of the total losses results from severe weather conditions (figure 2), but the cause of some losses often remains unknown, especially if there are no survivors. So it is possible that more than one-third of the total losses may result from bad weather conditions.

This is why we concentrate our research on capsizings due to severe weather conditions. The main problem is high waves resulting from storms. Seas generated directly by the wind may be superposed on swell: long waves, rich in energy, which are left over from other storms many hours before.

In order to analyse capsizings due to waves, accurate modelling of the wave–ship interaction is necessary. Model tests can provide insight into the nature of capsizings, too, but they are quite expensive and do not allow for highly sophisticated analysis, unlike mathematical models.

 

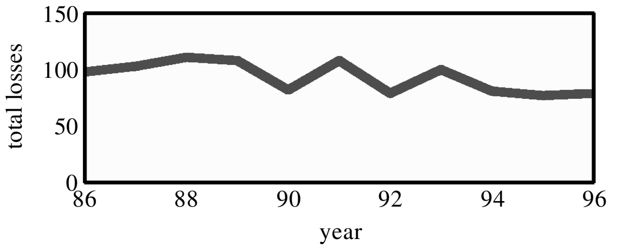


Figure 1. Number of actual total losses of ships over 500 GT, worldwide.

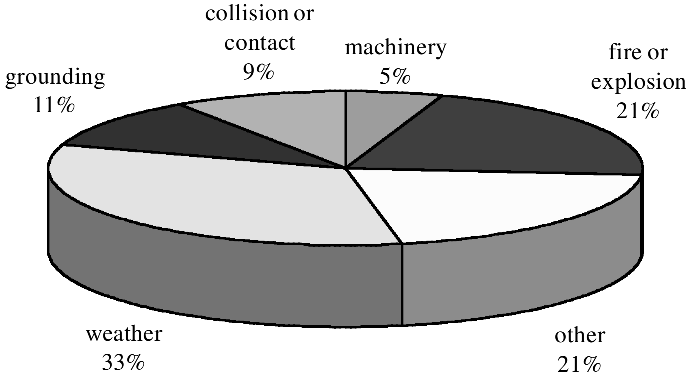


Figure 2. Causes of total losses 1986–1996.

In the past, several computer models have been developed. Because of the complexity of the problem, they were used to evaluate statistical properties (Petey 1988; Söding 1987). The probability of capsizing was estimated and heuristic arguments were used to interpret this probability and to derive stability criteria.

More advanced analysis techniques were recently applied to simple (Thompson 1997) and more complex (Spyrou 1996) computer models. These techniques are based on nonlinear dynamics theory. Using them, it is possible to locate stability boundaries. An overview of different analysis techniques is given in Baumgarten *et al.* (1997). The advanced analysis techniques, especially the path-continuation method (Allgower & Georg 1990), have been improved recently (Baumgarten 1999). We apply such techniques to advanced dynamic models for the motion of ships (Kreuzer & Wendt 1998, 2000).

## 2. Criteria and model test results

Current stability criteria are empirical and they are based on the properties of the righting lever (figure 3). The slope of the righting-lever curve at 0° is called the initial stability or metacentric height $GM$. National and international rules on intact stability make demands on minimum values and characteristics of the righting-lever curves (IMO 1995). These rules are accompanied by rules on damage stability (IMO 1997).

Model tests show that the current stability criteria do not always correlate with the danger of capsizing. At the Hamburg Ship Model Basin (HSMB), four different ship models were tested within an extensive test series (Blume & Hattendorff 1983,

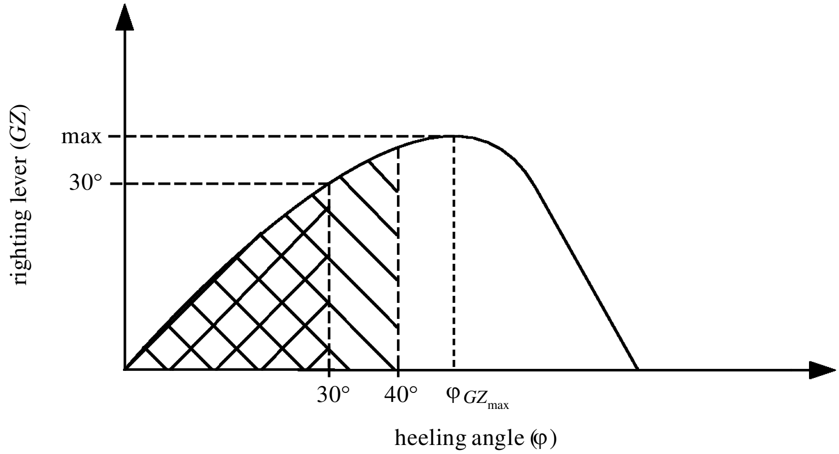


Figure 3. Righting-lever curve.

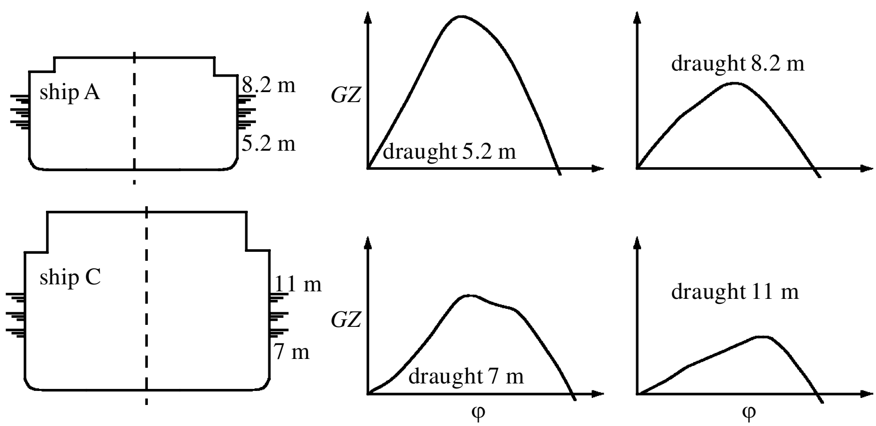


Figure 4. Righting-lever curves at the critical position of the centre of gravity for two ships at two different draughts.

1984). They were tested in following and quartering, irregular seaways. For each ship, the height of the centre of gravity was varied at a constant draught, and the corresponding righting-lever curves were calculated. This was done for three different draughts. The models capsized when the position of the centre of gravity passed a critical value. The righting-lever curves corresponding to the critical position were compared. The results showed that the acceptable righting-lever curves are very different for each ship and each draught. Examples are given in figure 4. Here, the righting-lever curves of the critical position of the centre of gravity are shown for two different ships and two different draughts each. The midship section of the two ships (ship A, ship C) is sketched and the waterlines of three different draughts are indicated.

Since the characteristics of the righting-lever curves at the critical position are very different, criteria based exclusively on these static curves are inadequate for the dynamic problem. From the model tests, a criterion was derived that combines hull characteristics and the draught with the old criteria, i.e. the righting-lever curves should be multiplied by a factor $C$ (Blume & Hattendorff 1983, 1984),

$$C = \frac{TD'}{B^2}\frac{C_B}{C_W}\sqrt{\frac{d}{KG}}\sqrt{\frac{100}{L}},$$

before being compared with the characteristics of the curve shown in figure 3. Different correlations are considered: large ratios of width:draught $(B/d)$ and width:depth $(B/D')$ decrease the range of stability $(\varphi(GZ = 0))$. Large ratios of $C_W : C_B$ are not welcome as they cause large variations of the righting moment. $C_B$ is the block coefficient, a measure of fineness with respect to the volume; and $C_W$ is the waterline coefficient, a measure of fineness of the waterplane area. From figure 4 we know that ships with small draught $d$ are more likely to capsize. The factor $\sqrt{d/KG}$ is a measure of this connection, where $KG$ is the height of the centre of gravity. Furthermore, the factor $C$ depends on the length $L$ of the ship. The longer the ship is, the larger the absolute stability values should be.

This criterion, however, lacks general applicability. It is derived from model tests with four ships of similar type. For a new type of ship, new model tests would have to be performed in order to adjust the criteria.

On the other hand, one should ask if it is useful to try to apply every new result as a factor on the old criteria. In order to overcome these shortcomings, we should find new characteristic values if we consider new physical aspects. Consequently, we aim to develop a criterion based on dynamic calculations.

## 3. Mathematical modelling of large-ship motions

### (a) Overview

As model tests are too expensive, it is necessary to analyse numerical models. There are many different ways of modelling the motions of ships. They may be subdivided into groups depending on their number of degrees of freedom, on the method of determination of their hydrodynamic forces, and on the description of the hydrodynamic and the hydrostatic forces, either spacial or planar.

One-degree-of-freedom models can be used to show certain general effects. In reality, all six degrees of freedom of the rigid body are coupled due to hydrodynamic and hydrostatic forces. For quartering seas, in particular, the coupling allows energy transfer between the six degrees of freedom.

Hydrodynamic forces can be determined by numerical discretization methods, such as boundary-element methods and singularity methods. Finite-element formulations are not common as the system's equations would become very large. Boundary-element methods seem to be the most promising for the modelling of large motions as there are no limitations on nonlinearities. Three-dimensional boundary-element models are still under development and are still restricted to relatively simple floating-body geometries. Singularity methods are easier to apply and are, therefore, the most common method used in practice. They have been developed for two- and three-dimensional problems. Different types of singularity methods take into account different phenomena, such as non-uniform flow around the hull, or memory effects. Usually, singularity methods are valid only for small motions.

Depending on the determination of the hydrodynamic forces, the state-space formulation can be of much higher dimension than the number of degrees of freedom

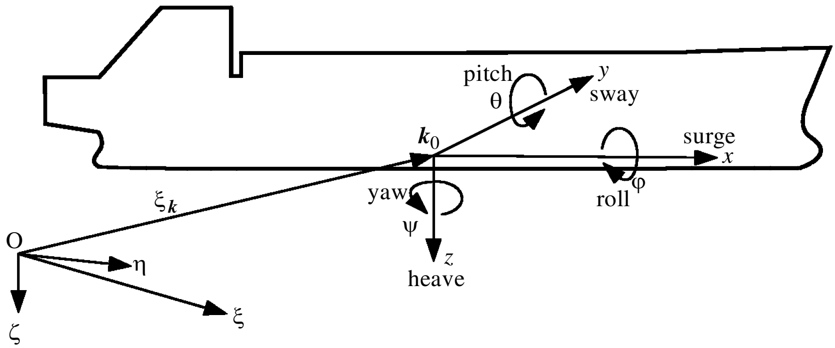


Figure 5. Inertial reference frame and coordinate system fixed with the ship.

multiplied by two. For boundary-element methods, the dimension depends on the number of boundary elements. For singularity methods, it depends on the number of additional equations that consider memory effects of the fluid.

In our approach, we consider the ship to be rigid, to avoid an unnecessarily complicated model, taking into account all six degrees of freedom as well as all couplings due to fluid–structure interactions. The hydrodynamic forces are calculated using a two-dimensional singularity method, as this is the most reliable approach currently available. Memory effects are taken into account, so that the dimension of the state-space formulation rises up to 164 degrees of freedom (the model is described in detail below). The computer code, called Simbel, was developed at Marinetechnik GmbH, Hamburg (Pereira 1988). We explain how the singularity-method restriction on small motions is overcome with this code in § 5 below.

For assessment purposes, and to evaluate the restrictions of the two-dimensional singularity method, we use another model, called Splash, developed at South Bay Simulations, Babylon, New York, USA. Using Splash we can calculate the hydrodynamic forces by considering the three-dimensional effects including non-uniform flow (see Kreuzer & Wendt 2000).

### (*b*) *Modelling with* Simbel

We combine Newton's and Euler's equations to describe the ship as a rigid body with six degrees of freedom,

$$\boldsymbol{M}\ddot{\boldsymbol{y}} + \boldsymbol{k}(\boldsymbol{y}, \dot{\boldsymbol{y}}, t) = \boldsymbol{q}(\boldsymbol{y}, \dot{\boldsymbol{y}}, t), \tag{3.1}$$

where $\boldsymbol{M}$ is the $6 \times 6$ inertia matrix, $\boldsymbol{q}$ is the vector of applied forces, and $\boldsymbol{k}$ is the vector of all internal forces. The vector of applied forces and moments, $\boldsymbol{q}$, collects all external forces acting on the ship. They result from forces due to radiation and diffraction, head and beam resistance, hydrostatic forces, forces due to the incident waves, forces due to the steady wave resulting from the forward speed, forces due to propulsion, forces due to the rudder, and gravitational forces. It is assumed that none of these components influences each other directly, and, hence, that the principle of superposition holds. The coordinate systems in figure 5 are used to describe the ship's position and orientation.

Most effort was necessary to obtain the radiation and diffraction forces. They are obtained from a hydrodynamic analysis of a number of cross-sections (strips) that

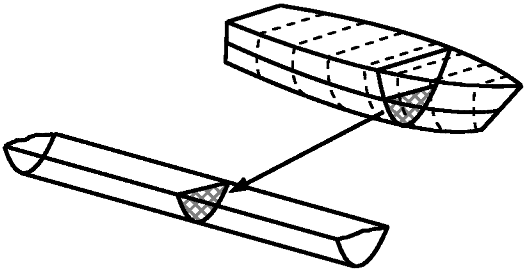

Figure 6. Strip theory.

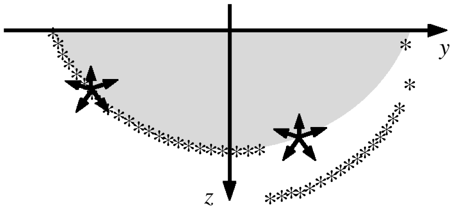


Figure 7. Sources along the boundaries of a cross-section.

represent small portions of the ship. Later, the strips are all joined together by compatible boundary conditions, and the forces on the complete system are integrated. It is assumed that the ship is slender, the hull is rigid, the speed is moderate, the motions are small, and the water is deep. It can then be assumed that the local hydrodynamic properties are the same as would be experienced if the strip was part of an infinitely long cylinder of the same cross-sectional shape, as shown in figure 6. That means that some three-dimensional effects, such as mutual interference of strips, are ignored (Lloyd 1989). Other three-dimensional effects, such as the variation of the shape over the ship's length, are taken into account. The hydrodynamic moments acting on the full ship in the pitch and yaw directions can be obtained from the heave and sway forces on the single strips. For the sway direction, however, the hydrodynamic forces cannot be evaluated by strip theory.

For the determination of the local hydrodynamic properties, fictitious two-dimensional sources are distributed along the boundaries of the strips (figure 7). These sources implicitly fulfil Laplace's equation (conservation of mass), which holds for an incompressible, inviscid, irrotational and homogeneous fluid (potential theory). The strengths of the sources—and, thereby, the potential of the flow—are determined for each strip, so that linearized boundary conditions are fulfilled (Yeung 1974). There are two kinematic boundary conditions: (1) that no water penetrates the hull; and (2) that no water penetrates the free surface. Further, there is one dynamic boundary condition: that the pressure at the free surface equals the atmospheric pressure. This condition is derived from Bernoulli's equation (conservation of momentum), which is the second governing equation that holds for the fluid. The ship is assumed to move periodically with fixed frequency and with small motions. How these restrictions are overcome is described later. The problem is solved using pulsating sources. From the strengths of the pulsating sources, the periodical forces acting on the hull are determined. Thereby, the radiation problem is solved. The waves produced by the periodic motion of the ship's hull produce forces that act back on the ship's hull. These are called radiation forces.

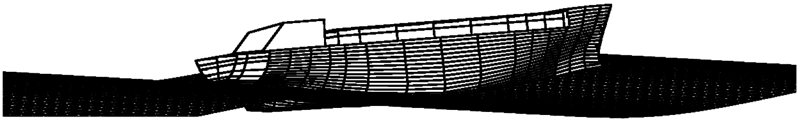

Figure 8. Discretizaton of the hull of the container ship 'ship C' for the calculation of the hydrostatic pressure.

The radiation forces depend linearly on the ship's acceleration and velocity. The amplitudes—the coefficients of the acceleration and velocity—are called added-mass and damping coefficients. It has to be mentioned that they are frequency dependent. In order to perform time-domain simulations, they are transformed to the time domain. For every cross-section, the added-mass and damping coefficients are approximated by polynomials in the frequency domain (Baumgarten *et al.* 1997; Pereira 1988). An inverse Laplace transformation yields a linear system of state equations (state model):

$$\dot{\boldsymbol{s}}(t) = \boldsymbol{f}(\boldsymbol{s}(t), \dot{\boldsymbol{u}}(t)). \tag{3.2}$$

Here, $\boldsymbol{f}$ is a function of the state vector $\boldsymbol{s}$ and the ship's absolute velocity $\dot{\boldsymbol{u}}(t)$. The dimension of the system depends on the order of the polynomial in the approximation and on the number of cross-sections. Finally, all the strips are joined together by compatible boundary conditions and the forces for the complete system are integrated along the ship's length.

The diffraction forces are caused by the perturbation of the incoming wave due to the presence of the hull. They are calculated implicitly with the radiation forces using the so-called concept of relative velocities. One imagines not that the ship is fixed in an external wave, but vice versa: that the ship moves with the velocity of the external wave and no external wave is present. The waves radiated by the ship in exactly these conditions are supposed to be the same as those generated by the perturbation of the incoming wave. Superposing the forces of radiation and this kind of diffraction, one can insert the relative velocity between the strip and the surrounding water instead of inserting the absolute velocity $\dot{\boldsymbol{u}}(t)$ into the state model (3.2) for the radiation forces.

The hydrostatic forces, as well as the forces due to the incident wave and the forces due to the steady wave resulting from the forward speed, are calculated under so-called hydrostatic assumptions. The ship is represented by a finite number of panels (figure 8). The forces are calculated for the ship fixed quasi-statically in the wave: for each corner point of each panel, the 'hydrostatic' pressure $p = \rho g h$ is calculated, where $\rho$ is the density and $g$ is the acceleration due to gravity. The height $h$ depends on the position of the point on the ship's hull, the height of the incoming wave, and the height of the steady wave resulting from the forward speed, which is approximated depending on the length of the ship and the Froude number $Fr$. This is a non-dimensional number relating inertial forces to gravitational forces. It corresponds to the forward speed $v$, $Fr = v/\sqrt{gL}$, where $L$ is a characteristic length, typically the length of the ship. After calculation of a mean pressure for each panel, the pressure is integrated over the wetted surface of the ship to obtain the forces and moments acting on the ship. Thus, the restoring and exciting forces and moments are determined from the momentarily wetted hull.




MATHEMATICAL, PHYSICAL & ENGINEERING SCIENCES
THE ROYAL SOCIETY A
PHILOSOPHICAL TRANSACTIONS OF

Figure 9. Ship C.

An additional roll damping moment $d$, resulting from viscous forces, is described by a linear and a quadratic term: $d = b_1\dot{\psi} + b_2\dot{\psi}|\dot{\psi}|$, where $\dot{\psi}$ is the roll velocity, and $b_1$ and $b_2$ are coefficients that were determined from model tests (Blume 1979).

After integration of the equations of motion using a Runge–Kutta scheme, time histories are obtained. The numerical results were compared with the results from a model test (Pereira & Söding 1990) and were found to represent the model behaviour acceptably accurately.

## 4. Modelling of real ships

In our analysis, we try to model reality as closely as possible, which is why we chose two vessels that were actually built for the analysis (see § 2). The model tests at the HSMB were done using models of these vessels. Using the nomenclature of the HSMB, we call them ship A and ship C. Ship A is a combined grain and container carrier, ship C carries containers only. Figure 9 is an elevation drawing of ship C. Ship A is similar, but its height:width ratio is smaller and its hatchways are lower.

Ship A is 145 m long (overall), 23 m wide and 11 m high. Its mean draught is 8 m, it has a displacement of 17 800 t, and its gross tonnage is 8750. Ship C is 169 m long, 28 m wide and 16 m high, its mean draught is 10 m, its displacement is 29 300 t, and its gross tonnage is 19 193.

For the hydrostatic calculations, the surfaces of both ships' hulls were discretized by panels to calculate the hydrostatic pressure on the hull (cf. figure 8). For the hydrodynamic calculations, ship A was divided into 22 cross-sections, ship C into 24. The distance between the chosen cross-sections at the bow and at the stern is smaller than at midship, because the shape of the sections varies only a little there.

At each cross-section, the frequency-dependent hydrodynamic masses and dampings were calculated for different draughts and heelings in 344 combinations: eight different heelings, varying between 0 and 70°, 43 different draughts, varying from 0 m upwards in steps of 0.5 m. For each section–draught–heeling combination, the frequency-dependent hydrodynamic masses and dampings were approximated by polynomials of second order to allow a transformation of the frequency-dependent forces to the time domain. For the coefficients of the polynomials, six $3 \times 3$ matrices for each combination were needed. That means that $18\,576 \times 22 = 408\,672$ values for ship A and $18\,576 \times 24 = 445\,824$ values for ship C were stored to be used later for the calculation of the hydrodynamic forces.

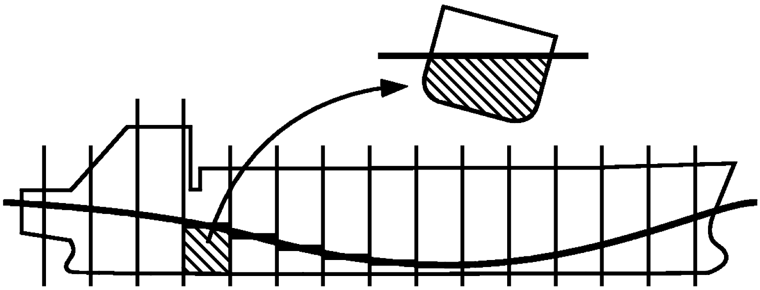

Figure 10. Division of the ship into sections; the selection of sections depends on the position of the ship in the wave.

## 5. Nonlinear aspects in the mathematical model

The nonlinearities of the mathematical model for the ship motion are described here. 'Nonlinear' means nonlinear dependence of the function $\dot{\boldsymbol{x}} = \boldsymbol{f}(\boldsymbol{x})$ on the state variables $\boldsymbol{x}$. In contrast to that in computational fluid dynamics, the term 'nonlinear' denotes nonlinear boundary conditions of steady or unsteady flow. There, the dependence of the fluid boundary conditions on the velocities of the fluid is nonlinear. In the steady case, only a constant steady motion, and no body oscillations, is considered.

In our model, two main parts make the differential equation nonlinear: the hydrostatic forces and the hydrodynamic forces.

### (*a*) *Nonlinearities due to hydrostatics*

The hydrostatic forces, which are usually the restoring terms, depend nonlinearly on the position, a part of the state vector. In our case, we consider not only the dependence on the roll angle (righting-lever curve) but also on the heave displacement and on the pitch angle. The hydrostatic pressure at many points on the wetted portion of the hull (figure 8) and the corresponding forces are calculated in each time-step, depending on the ship's position and orientation.

Furthermore, the calculation of the hydrostatic pressure takes into account the dependence on the wave elevation of the water surface. This does not make the differential equation nonlinear; it represents the excitation due to the wave.

### (*b*) *Nonlinearities due to hydrodynamics*

The calculation of the hydrodynamic forces due to radiation and diffraction is based on the assumption of small oscillations in all known codes used to calculate ships' motions, including SIMBEL. In SIMBEL, however, the calculation is approximated for large-ship motions in all degrees of freedom. This means that the coefficients of the polynomials describing the added masses and dampings in the state equation are not constant. Depending on the position of the ship in the wave, the fitting coefficients are chosen from a table. This is sketched in figure 10.

In each time-step, the actual draught and heeling of each section is determined, depending on the position of the ship and on the height of the wave at the section in question. As mentioned in § 4, the polynomial coefficients were calculated for ships A and C for 344 different draught–heeling combinations for each section. The combination that best fits the actual draught and heeling of the section is selected

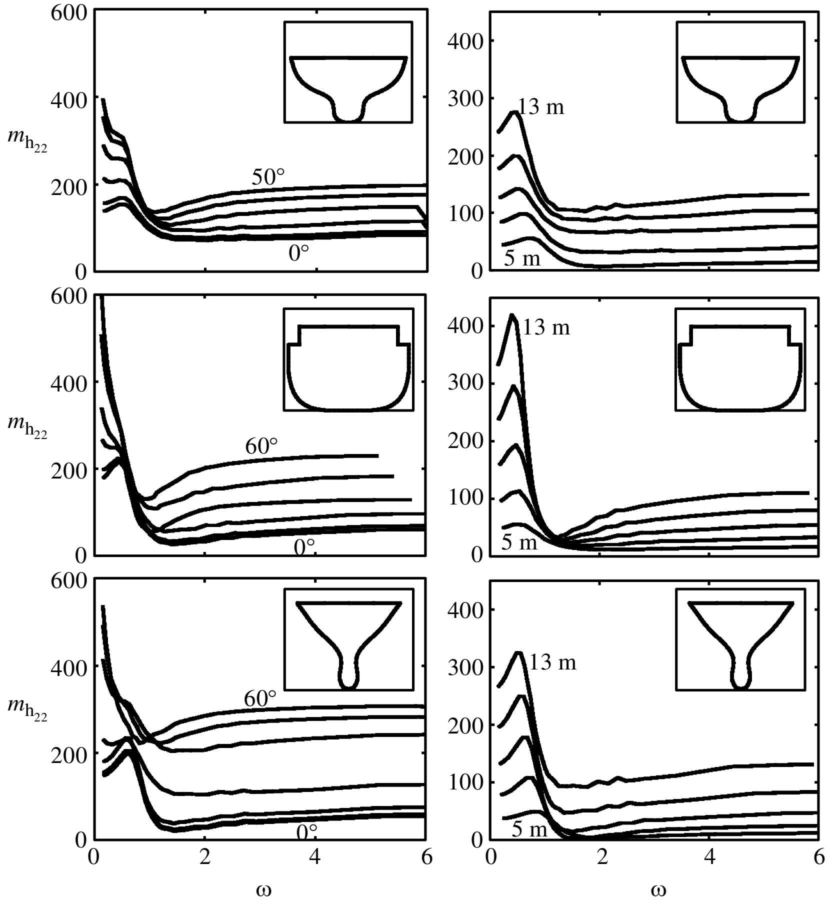


Figure 11. Hydrodynamic mass $m_{h22}$ (sway direction) depending on the frequency $\omega$ at different sections of ship C (left column) with variation of heeling (draught = 9.5 m) and (right column) with variation of draught (heeling = 0°). Top row 16 m, middle row 48 m and bottom row 150 m beyond after perpendicular.

and the corresponding coefficients are used in the time integration. Thus, by switching between the coefficients during the integration, one can take into account the nonlinear dependence of the radiation/diffraction forces on the position.

Figure 11 shows how the hydrodynamic masses change with the position. Only the element in row 1, column 1 of the $3 \times 3$ added-mass matrix is shown. The element stands for the force in sway direction when the section is oscillating in the same direction. Its frequency-dependent values are shown at three different sections, one near the bow (16 m beyond after perpendicular), one at midship (48 m beyond after perpendicular), and one near the stern (150 m beyond after perpendicular). In the first column, the values are shown for variation of the heeling at a constant draught of 9.5 m; in the second, the values are shown for variation of the draught at a constant heeling of 0°. Changes of the hydrodynamic mass and damping coefficients with variations like these cause additional nonlinearities in the differential equation.




PHILOSOPHICAL TRANSACTIONS OF THE ROYAL SOCIETY A MATHEMATICAL, PHYSICAL & ENGINEERING SCIENCES

## 6. Simulations and nonlinear phenomena

Simulations were done to represent different seaways. We concentrated on simulations of regular seas, since there we can observe nonlinear phenomena at best. We are free to vary wave height $H$, period $T$, and heading angle $\mu$.

Ships travelling in rough seas are likely to encounter various kinds of dangerous phenomena, which may lead to capsize. Most dangerous are following and quartering seas, according to accounts of masters. In both sea states, the waves come from behind: following seas come from directly behind the ship, quartering seas strike the ship obliquely from behind. In such seas, the metacentric height $GM$—the slope of the righting-lever curve at 0°—varies. This variation can cause parametric excitations. Furthermore, phenomena like surf-riding and broaching can occur. Therefore, simulations were made for following and quartering seas for different wave heights. The calculations described below were done for ship C, with a speed of *ca.* $v_{\text{ship}} = 11\ \text{m s}^{-1}$, and a draught of $d = 9.32$ m, which corresponds to a typical loading condition.

### (a) *Simulations of the ship's motion in following seas*

Simulations of the ship's motion in following seas (heading angle $\mu = 0°$) were performed with fixed rudder while the ship was free to yaw. Small perturbations induce yaw and roll motions. This is probably due to parametric excitation. Figure 12 shows the time histories and phase portraits of the roll motion after the transient response vanished. The time histories show that the roll amplitude is small for wave heights up to 9 m. The amplitude increases rapidly for slightly higher waves. This leads to capsize at wave heights of 10 m. More details can be obtained from the phase portraits of the motion. They show that the capsize of the ship at 10 m is the result of a sequence of bifurcations, qualitative changes of the dynamic behaviour, caused by varying at least one system parameter. For different wave heights one-periodic, two-periodic, chaotic, and three-periodic orbits can be observed separated by bifurcations. A last bifurcation leads to capsize: for $H = 10$ m, there exists no stable motion in an upright position. From these results it is obvious that the nonlinear model cannot be replaced by a linear one. Bifurcations in roll motion correspond to other bifurcations, e.g. bifurcations in heave and pitch. This shows that a coupling between heave, pitch and roll exists.

A sequence of images of the ship in the wave is shown in figure 13. One can see that the pitch motion is large, but that roll motion is also visible, though there are only small perturbations inducing this motion. An animation can be found at http://www.mt2.tu-harburg.de/mwendt.

### (b) *Simulations of the ship motion in quartering seas*

Contrary to the simulations of following seas, the wave frequency for quartering-seas simulations was not set constant. In nearly all sea areas, the significant wave period correlates with the wave heights. This was considered in the simulations of quartering seas. The stronger the wind blows, the higher and longer the waves become. The correlation is shown in figure 14 for the North Sea, with values taken from Hattendorff (1974).

MATHEMATICAL, PHYSICAL & ENGINEERING SCIENCES
PHILOSOPHICAL TRANSACTIONS OF THE ROYAL SOCIETY A

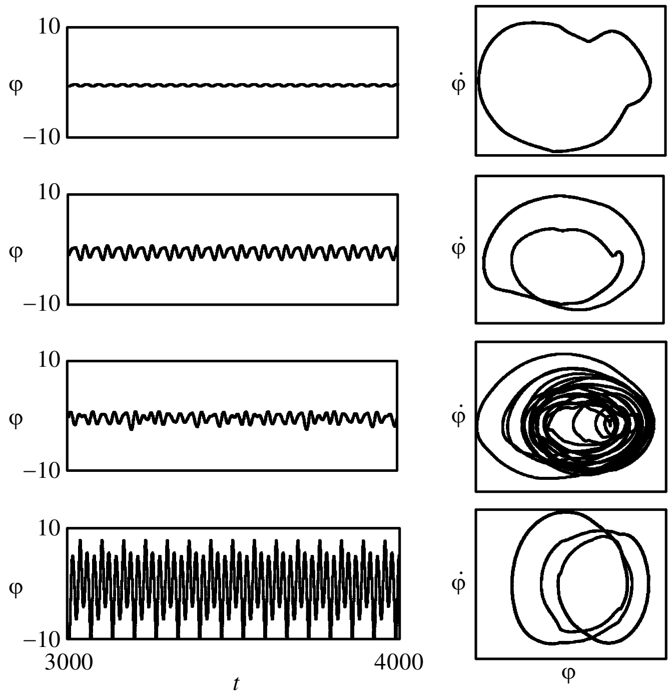


Figure 12. Time histories ($\varphi$ versus $t$, $\Delta t = 1000$ s) and phase portraits ($\dot{\varphi}$ versus $\varphi$) of the roll motion (roll angle $\varphi$) of ship C travelling with speed $v_{\text{ship}} = 11$ m s$^{-1}$ in a following sea ($\mu = 0°$) at a wave frequency of $\omega = 0.5$ s$^{-1}$ and wave heights of $H = 2.0$ m, 8.0 m, 9.0 m and 9.6 m.

Figure 13. Ship C in following seas, with wave heights of $H = 9.8$ m. The rudder is fixed but the ship is free to yaw, so that the heading angle varies around $\mu = 0°$.

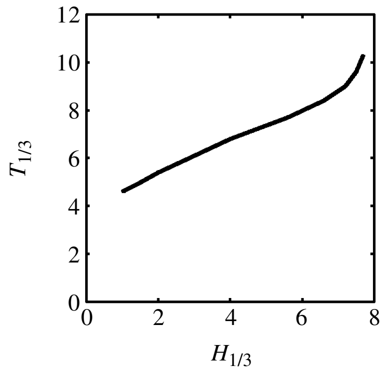


Figure 14. Significant wave period $T_{1/3}$ correlates with significant wave heights $H_{1/3}$. This correlation is valid for the North Sea.

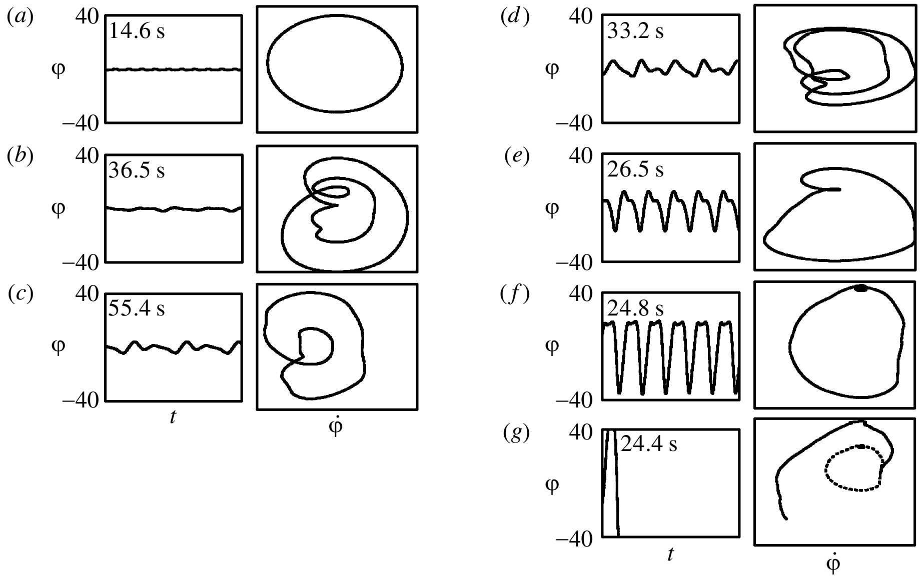


Figure 15. Time histories ($\varphi$ versus $t$, $\Delta t = 146$ s) and phase portraits ($\varphi$ versus $\dot{\varphi}$) of the roll motion (roll angle $\varphi$) in quartering sea ($\mu = 30°$) with fixed yaw angle at wave heights of $H = 1$ m (*a*), 2 m (*b*), 4 m (*c*), 6 m (*d*), 8 m (*e*), 10 m (*f*) and 12 m (*g*). The dashed line in the phase portrait for $H = 12$ m indicates the periodic motion at $H = 10$ m from which the system escapes when the wave height increases. The number within the graphs is the encounter period $T_e$.

In order to consider the correlation between wave period and wave height, the curve in figure 14 was approximated by a linear equation: $T = 4.6\,\mathrm{s} + 0.7(H - 1\,\mathrm{m})\,\mathrm{s\,m^{-1}}$. For the simulations of quartering seas (heading angle $\mu = 30°$), the wave period was changed together with the wave height according to the approximation.

Two different types of yaw control were used. In the first series of simulations, the yaw angle was fixed (constraint). Figure 15 shows the corresponding time histories and phase portraits of the roll motion. Small waves are slower than the ship ($v_{\mathrm{ship}} = 11\,\mathrm{m\,s^{-1}}$) and large waves overtake the ship. This is due to the fact that the wave phase velocity is inversely proportional to the frequency, in combination with the correlation between wave frequency and wave height. At $H = 3$ m, the encounter frequency $\omega_e = \omega - (\omega^2 v_{\mathrm{ship}} \cos\mu)/g$ is nearly zero. These simulations show that for wave heights near 3 m, two-periodic motions exist. The bifurcations between the states shown are probably not due to the variation of the wave heights, but to the extreme variations in the encounter frequency. For high waves, the motions are again one-periodic. For waves higher than 10 m, the ship capsizes.

Another series of simulations was performed with free yaw angle. For quartering seas and free yaw angle, an active rudder control is necessary. Otherwise, the ship cannot keep the heading. In SIMBEL, a proportional integral-differential rudder control is implemented. It was used for the simulations shown in figures 16 and 17.

The simulations show that the ship will capsize much earlier if the yaw angle is free instead of fixed. At a wave height of 6 m, the controller is not able to maintain the heading any more (figure 17). The sequence of images in figure 18 shows the last

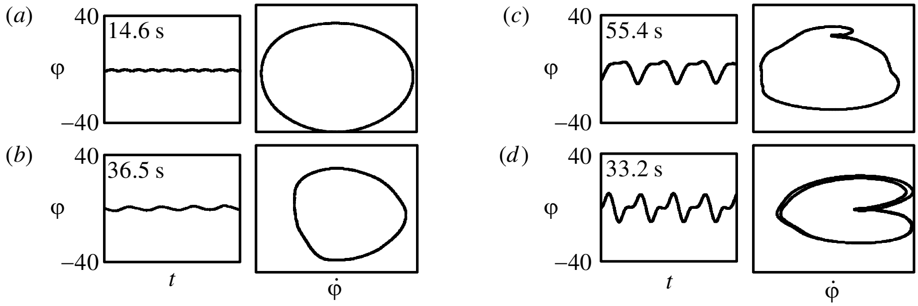


Figure 16. Time histories ($\varphi$ versus $t$, $\Delta t = 146$ s) and phase portraits ($\varphi$ versus $\dot{\varphi}$) of the roll motion (roll angle $\varphi$) in a quartering sea ($\mu = 30°$) with free yaw angle at wave heights of $H = 1$ m (*a*), 2 m (*b*), 4 m (*c*) and 5 m (*d*).

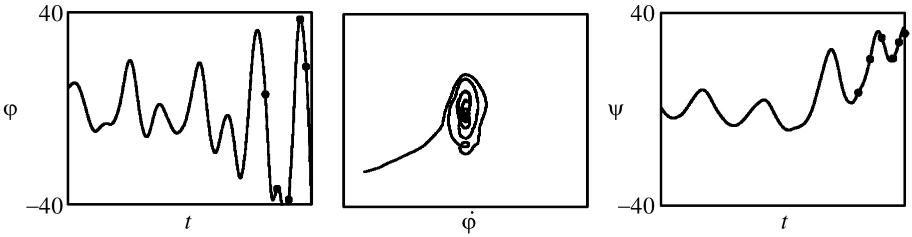


Figure 17. Time histories ($\varphi$ versus $t$, $\Delta t = 150$ s) and phase portraits ($\varphi$ versus $\dot{\varphi}$) of the roll motion (roll angle $\varphi$) and time history ($\psi$ versus $t$) of the yaw motion (yaw angle $\psi$) in a quartering sea ($\mu = 30°$) with free yaw angle at a wave height of $H = 6$ m.

30 s of the motion. While broaching, the amplitude of the roll angle grows and the ship eventually capsizes.

This observation corresponds to observations made by masters. Model tests with models of ships A and C in irregular seaways show the same phenomena (Blume & Hattendorff 1983, 1984). Often, capsize was preceded by a deviation in the heading (broaching). Unfortunately, no model tests in regular seaways were carried out. Thus, a direct comparison between the computer simulation and the model tests is not possible. Also, Spyrou & Bishop (1999) observed the broaching phenomenon using computer simulations. They mentioned that the region of stability depends on the control parameters. This is understandable: the better the quality of the control, the better the ship will keep its heading. Only when broaching does the situation become dangerous and capsize becomes possible.

Another interesting observation can be obtained from figure 16. In the phase portrait of the motion at $H = 5$ m, a two-periodic orbit is visible. As in the simulations of following seas, a bifurcation can be found before the ship capsizes. It can be considered as an indication that a dangerous situation might arise.

### (*c*) *Areas of uncertainty*

Although simulations using SIMBEL showed good general agreement with model tests (Pereira & Söding 1990), errors are always possible in simulations. Small errors might occur when switching between the radiation coefficients (see § 5) as this is an abrupt event. Other small errors might result from neglecting some three-dimensional

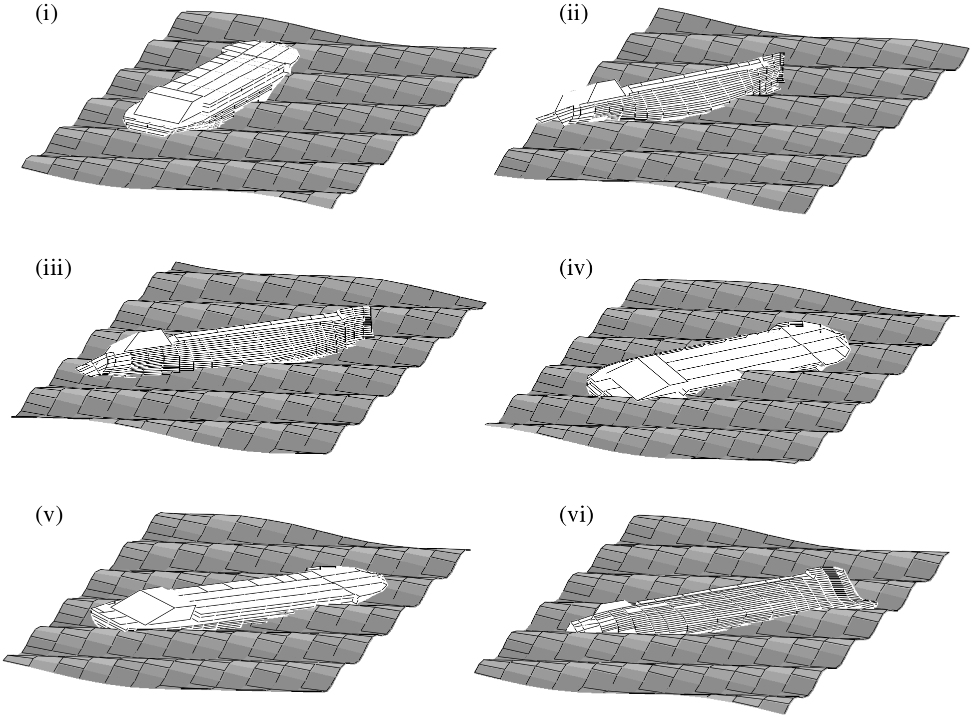

Figure 18. Ship C in quartering seas, with a wave height of $H = 6$ m. The images are drawn for the moments indicated by the dots in figure 17.

effects, but these effects are small for slender ships like the ones under consideration here. Another cause of faults might be the approximation of beam and heave resistance. Especially for large yaw motion, e.g. broaching, a correct beam resistance of all the sections is important. Furthermore, the determination of the additional roll damping moment is not exact. It is approximated from non-dimensionalized measurements of other vessels. An important problem might be the very small encounter frequency in the simulations with $H = 4$ m. For very small frequencies, the hydrodynamic coefficients and the approximated polynomials are not reliable.

In order to be certain about the results, specific model tests would have to be performed. Some comparisons between available experimental data and simulations for ship A were done with positive results. To obtain absolute certainty about the simulations presented here, however, one would need model tests under exactly the same conditions. They are not currently available.

## 7. Concluding remarks

The current stability criteria for ships are not sufficient to assess a ship's stability reliably. Each year, ocean vessels are lost in severe weather conditions. A detailed analysis of the dynamics of each ship is necessary to provide criteria to prevent it from capsizing.

Advanced mathematical modelling is necessary to describe a ship's dynamics as accurately as possible, so that all important effects are accounted for. We use a model that describes the ship's six rigid-body degrees of freedom and their couplings. This is necessary as dangerous situations usually involve all of these degrees of freedom. The model includes the dependence of the hydrodynamic coefficients on the frequency. This leads to many additional state equations. Furthermore, the dependence of the hydrostatic and the hydrodynamic forces on the state variables is described as nonlinear.

Using this model, simulations were done. They showed that the coupling of the degrees of freedom is important for the description of capsizing scenarios. For example, in back quartering seas, the ship broaches before capsizing. In the simulations with fixed yaw angle (constraint), the ship resists much higher waves.

Another interesting observation is that bifurcations occur before the ship capsizes. When the ship is free running, there is always at least one bifurcation indicating that the ship will capsize. That is why we concentrate on the detection of such bifurcations. The application of path-following methods to determine bifurcations is under development. They allow systematic detection of critical conditions.

This work was supported by the DFG (Deutsche Forschungsgemeinschaft, i.e. German Research Foundation) under contract Kr 752/16-2. We thank Marinetechnik GmbH, Hamburg, for providing us with the software SIMBEL, and R. Pereira for his assistance in using it.

## References

Allgower E. L. & Georg K. 1990 *Numerical continuation methods*. Springer.

Baumgarten, R. 1999 *Dynamisches Nachbeulverhalten parametrisch erregter, dünnwandiger Schalenfelder*. Fortschr.-Ber. VDI, series 1, no. 314. Düsseldorf: VDI Verlag.

Baumgarten, R., Kreuzer, E. & Wendt, M. 1997 Nonlinear dynamics in marine technology. *Eur. J. Mech.* A/*Solids* **16**, 25–44.

Blume, P. 1979 Experimentelle Bestimmung der Koeffizienten der wirksamen Rolldämpfung und ihre Anwendung zur Abschätzung extremer Rollwinkel. *Schiffstechnik* **26**, 3–23.

Blume, P. & Hattendorff, H. G. 1983 Stabilität und Kentersicherheit moderner Handelsschiffe. Berichte Nr. S 165/83, S 178/83. Hamburgische Schiffbau-Versuchsanstalt, Hamburg.

Blume, P. & Hattendorff, H. G. 1984 Stabilität und Kentersicherheit moderner Handelsschiffe. Berichte Nr. S 184/84. Hamburgische Schiffbau-Versuchsanstalt, Hamburg.

Hattendorff, H. G. 1974 Seeverhalten. *Handbuch der Werften* **12**, 180–219.

IMO 1995 *Code on intact stability for all types of ships covered by IMO instruments*. Resolution A.749(18). London: International Maritime Organization.

IMO 1997 *SOLAS*, Consolidated Edition. Consolidated text of the International Convention for the Safety of Life at Sea, 1974, and its Protocol of 1978: articles, annexes and certificates. Incorporating all amendments in effect from 1 July 1997. London: International Maritime Organization.

Kreuzer, E. & Wendt, M. 1998 Stabilität von Schiffsbewegungen. *Z. Angew. Math. Mech.* **72**, S561–S562.

Kreuzer, E. & Wendt, M. 2000 Ship capsizing as a nonlinear dynamics problem. In *IUTAM/IFToMM Symp. on Synthesis of Nonlinear Dynamical Systems*, pp. 37–48. Dordrecht: Kluwer.

Lloyd, A. R. J. M. 1989 *Seakeeping: ship behaviour in rough weather*, 1st edn. Chichester: Ellis Horwood.

Pereira, R. 1988 Simulation nichtlinearer Seegangslasten. *Schiffstechnik* **35**, 173–193.

Pereira, R. & Söding, H. 1990 Simulation der Schiffsbelastungen im Seegang. Abschlußbericht zum BMFT-Vorhaben MTK 0440 B. Hamburg: Institut für Schiffbau der Universität Hamburg.

Petey, F. 1988 Ermittlung der Kentersicherheit lecker Schiffe im Seegang. *Schiffstechnik* **35**, 155–172.

Söding, H. 1987 Ermittlung der Kentergefahr aus Bewegungssimulationen. *Schiffstechnik* **34**, 28–39.

Spyrou, K. J. 1996 Dynamic instability in quartering seas: the behaviour of a ship during broaching. *J. Ship Res.* **40**, 46–59.

Spyrou, K. J. & Bishop, S. R. 1999 On the multi-degree, nonlinear dynamics of ship motions with application to the broaching problem. In *IUTAM Symp. New Applications of Nonlinear and Chaotic Dynamics in Mechanics*, pp. 417–424. Dordrecht: Kluwer.

The Institute of London Underwriters 1997 *Hull Casualty Statistics. IUMI Conf. Paris.* London: The Institute of London Underwriters.

Thompson, J. M. T. 1997 Designing against capsize in beam seas: recent advances and new insights. *Am. Soc. Mech. Engrs* **50**, 307–325.

Yeung, R. W. 1974 A singularity method for free-surface flow problems with an oscillating body. University of California, Berkeley, College of Engineering, report NA 73–6.